Numerical Simulations of Coupled Moisture and Heat Transfer in Wood during Kiln Drying: Influence of Material Nonlinearity

Pavlína Suchomelová,* Miroslav Trcala, and Jan Tippner

Finite element simulations of coupled thermal and moisture fields in wood during kiln drying were observed with a focus on non-isothermal moisture transfer in three-dimensional orthotropic models of wood with an initial moisture content below the fiber saturation point. Four different unsteady-state numerical models of the drying process were compared with the assumptions given by standards commonly used in wood kiln-drying processes. The first model describes linear simulation, and the other three models present nonlinear simulation using variable material coefficients dependent on temperature and moisture content, differing in settings of the Soret effect (thermodiffusion). A linear model was useful for predicting only the average moisture content during drying. Moreover, the nonlinear simulations were useful for computing the moisture content distribution. High differences (2.31% of moisture content) were found between the flow of moisture predicted by numerical models and standard requirements.

Keywords: Coupled heat and mass transfer; Material coefficients nonlinearity; Multiphysical modeling; Kiln-drying wood

Contact information: Department of Wood Science, Faculty of Forestry and Wood Technology, Mendel University in Brno, Zemědělská 3, 613 00, Brno, Czech Republic;
** Corresponding author: pavlina.suchomelova@mendelu.cz*

INTRODUCTION

Wood drying operations are an important part of lumber processing for use in the furniture or building industries. The quality of the drying process affects the final product quality, especially in terms of its physical and mechanical properties such as the dimensional stability, biodegradation resistance, or wood cracking. However, wood as a material shows significant property variability, and this adversely influences the drying process and dry timber quality (Pang 2007). The aim is to decrease drying time (and energy consumption) and the negative influences of drying on the properties of wood (Trcala 2015). One of the strategies on how to improve the process of wood drying is optimization of the drying schedule for different types of wood and for different requirements on the final product (Elustondo and Oliveira 2006). The drying and dry timber quality is affected by a wide range of factors, and thus it is costly and time consuming to experimentally investigate the influence of all these variables. Mathematical models have been recognized as a powerful tool to fulfil tasks of wood drying processes optimization (Pang 2004), and they can be also very useful for creating of drying schedules (Mitchell 2019) as well as for evaluation of stresses and cracks that arise during wood drying (Nascimento *et al.* 2019; Pérez-Pena *et al.* 2018) or for predicting of heat-mass transfer in wood during wood thermal modifications (He *et al.* 2019).

Wood drying is a dynamic process. It can be generally described as a coupled motion of the temperature and moisture fields with the local thermodynamic equilibrium in every point of the timber, reflecting the local changes of material coefficients depending on the mass and energy motion in the body (Gebhart 1993).

Kiln Drying of Wood

In terms of time and energy consumption, timber drying is one of the most demanding operations in wood processing (Elustondo and Oliveira 2006). The decreasing drying rate is compensated by continuous changes in the ambient temperature of drying (Jankowsky and Gonçalves Luiz 2006). Timber dries nonuniformly in its volume (Trcala 2012).

Convective kiln drying is the most commonly used method for sawn timber drying. The convectional kilns are designed to dry wood in the air and steam fusion, at the temperature of 40 °C (low-temperature seasoning and pre-drying) or temperatures of 40 to 100 °C (common hot-air drying) (Klement and Detvaj 2007; Perré and Keey 2007). As a good alternative to convective drying, superheated steam is also used as a drying medium (Kocaefe *et al.* 2007). Dehumidifier, vacuum, microwave, or solar kilns are other examples of wood drying (Perré and Keey 2007).

Modeling the Transport Processes in Wood

The numerical simulations of transport processes in wood are used as a tool for the mathematical and physical description of wood behavior in many aspects, such as building physics, behavior of wood-based composites, wood jointing, heat treatment of wood, or wood drying processes (Kang *et al.* 2008). The heat and mass modeling has progressed from the macroscopic description of these fields (Babiak 1995). The macroscopic model is based on the Fick's law of diffusion for the mass transfer and the Fourier's law for the heat transfer (Siau 1995). There are moisture concentration and temperature gradients in diffusion modeling, which are considered a moving force of the heat and mass transfer (Sherwood 1929; Vergnaud 1991). As a motion, the force of water diffusion in wood is sometimes used also as the water vapor partial pressure gradient (Siau 1984), where the air relative humidity (RH) influenced by actual moisture content in wood and temperature is observed. The multiphysical approach to the modeling of transport processes in wood seems to be the most appropriate to apply the thermodynamic models (Trcala 2012). The theory of coupled moisture and temperature fields motion is based on irreversible thermodynamic processes that were described by Luikov (1966) and Whitaker (1977).

Describing the bound moisture and temperature transfer in wood requires a comprehensive approach and the consideration of many physical phenomena. It is necessary to consider reciprocal influences of all the material coefficients and physical phenomena in coupled-fields modeling. Material properties of wood, such as density, diffusion coefficients, thermal conductivity coefficients, and specific heat, are dependent on the actual moisture content and temperature of wood (Horáček 2004). The weakness of most of the numerical models is their need for back-calculated material parameters without a clear physical meaning (Eitelberger and Hofstetter 2011).

The differences between full and partial nonlinearity of the heat and mass transfer in capillary-porous body were investigated by Lewis and Ferguson (1993). They compared two formulations of the Luikov equations (Luikov 1980). First, a fully nonlinear formulation with varying material properties, and second, a partially nonlinear formulation where some material properties were held constant. In the one-dimensional example

presented by Lewis and Ferguson (1993), the fully coupled model predicted the equilibrium achievement faster than the partial nonlinear model, but the difference was insignificant (Lewis and Ferguson 1993). This paper mainly presents a comparison of full nonlinear, partial nonlinear, and linear models of heat and mass transfer, regarding the Soret effect.

The heat and moisture transfer should be considered as coupled processes. The Soret effect (described by the thermodiffusion coefficient) is a moisture transfer induced by temperature gradient, and the Duffour effect expresses the heat flux induced by water diffusion (Siau 1984; Avramidis *et al.* 1992a).

It is not possible to use Fick's and Fourier's law separately, when modeling the wood drying processes. The multiphysical problem of water diffusion and heat transfer can be described by the system of two partial differential equations (PDEs), which is modified with relations to Soret and Duffour effects (Horáček 2004). When simulating the temperature and moisture fields during drying, the anisotropic or orthotropic properties of wood have to be considered (Trcala 2012).

Numerical models in this paper are focused on a convective hot-air kiln-drying of pre-dried timber. The study provides a comparison of numerical models using various settings of material parameters (different nonlinearity levels) and thermal-moisture fields couplings. Numerical solutions demonstrate that the settings of numerical model parameters and the coupling method can significantly influence simulation results, especially in its heating phase.

EXPERIMENTAL

Methods

The aim of the study was to determine the influence of nonlinearity of the material coefficients on the results of wood kiln-drying numerical models and to compare the results with commonly used standards for kiln-drying of wood (ON 49 0651 1989) used in central Europe.

The software *COMSOL Multiphysics* (COMSOL AB, version 5.4, Stockholm, Sweden), which is based on the finite element method (FEM), was used for numerical solution. This software provides an opportunity to imply own PDEs systems and own material models.

Four various transient numerical models were built and are described in Table 1. In the first model (*A*) all of the material coefficients were set as constants. Material coefficients that depend on actual moisture content and temperature were used in simulations B_1, B_2, and B_3.

Table 1. Description of Four Variants of Numerical Models

Numerical Model	Description
A	Linear computation with constant material coefficients
$\boldsymbol{B_1}$	Nonlinear computation with material coefficients dependent on moisture content and temperature, not affected by Soret effect
$\boldsymbol{B_2}$	Nonlinear computation with material coefficients dependent on moisture content and temperature, affected by constant Soret effect coefficient
$\boldsymbol{B_3}$	Nonlinear computation with material coefficients (including Soret effect coefficient) dependent on moisture content and temperature

For numerical modeling of wood drying processes it is necessary to define initial conditions, ambient parameters, boundary conditions, drying time, material coefficients of wood, and the region geometry. At the same time, it is important to consider the necessity of the simplification. These choices are important not only with respect to accurately modeling the real situation, but also to expressing the problem in a way that can be addressed using available computational software. This study includes the following: (i) the specially orthotropic homogenous body of dried timber; (ii) uniform initial moisture content and temperature in the timber; (iii) constant moisture and heat transfer coefficients; (iv) the Duffour effect negligence; and (v) negligence of the strain-stress effects.

The geometry of dried timber was represented by a solid block with dimensions of $2000 \times 200 \times 50$ mm^3, where the longitudinal (L), radial (R), and tangential (T) directions are identical with the solid's geometrical axes (specially orthotropic body). The location of the block into the Cartesian coordinate system is presented in Fig. 1

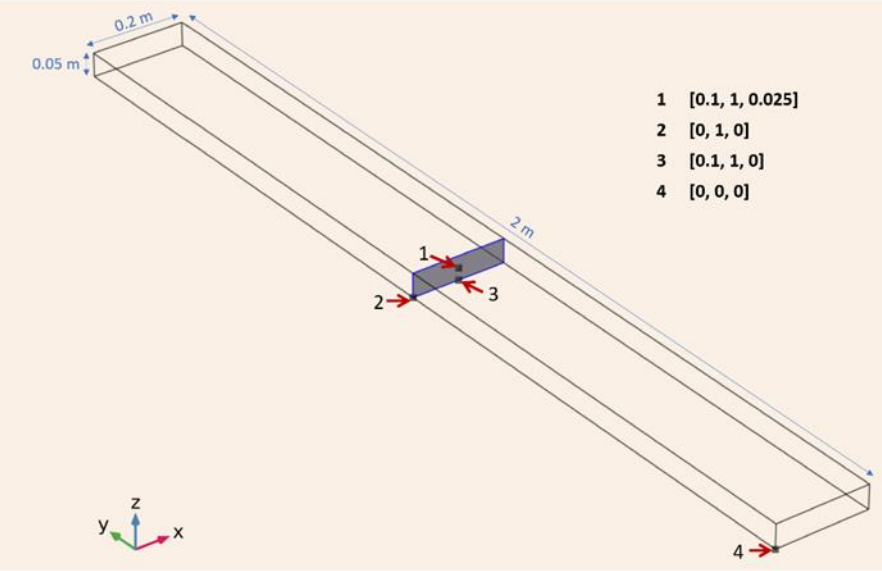

Fig. 1. Geometry and dimensions of the timber; location of the special orthotropic body into the Cartesian coordinate system used in the model (x = T, y = L, z = R), and position of points and area where the results were evaluated

The initial conditions were taken as uniform – constant in the whole volume. The initial moisture content value was lower than the fiber saturation point (M_0 = 25%), which corresponds to the moisture content of pre-dried timber. The uniform temperature of the timber at the drying process beginning was T_0 = 283 K.

The properties of drying ambient and total time are given by the drying schedule. To be able to compare results of numerical simulations, the drying schedule has to be designed in accordance with the standard for wood kiln-drying (ON 49 0651 1989). The drying schedule parameters were set for the usual timber with final moisture M = 8%. The ambient parameters as RH and equilibrium moisture content (*EMC*) are given by the standard. Both are functions of time (Fig. 2). The air velocity and drying temperature are uniform throughout the drying process (v_{air} = 1.5 m/s, T = 353 K).

Each numerical model of the wood block was observed at four different points and at the middle area for values of temperature and moisture content during the drying time. The average moisture content in the whole body was observed.

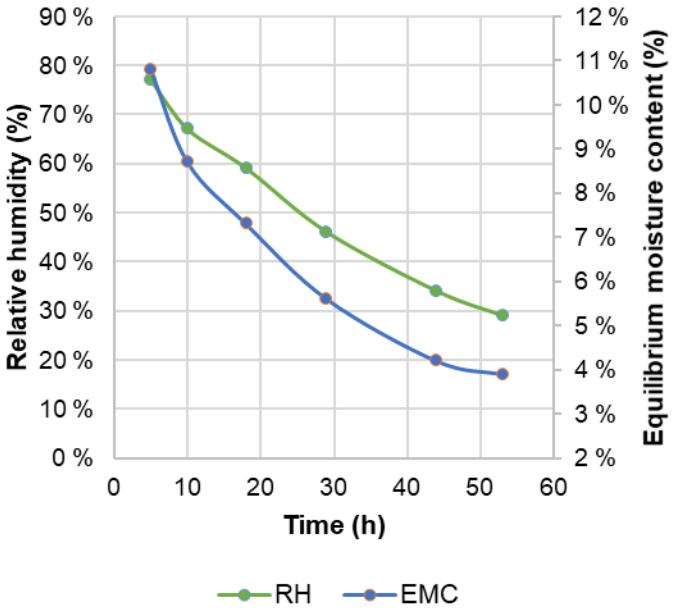

Fig. 2. Drying schedule parameters during drying process

Coupled PDE's Definition

The coupled transient modeling of the drying process is based on the system of two partial differential equations given by Siau (1992) and Avramidis *et al.* (1992b). The timber with an initial moisture content under the fiber saturation point contains the bound water. The motion of bound water is caused by diffusion. The main driving force of bound water diffusion is the moisture content gradient, but it is simultaneously influenced by the temperature gradient. Fick's law describes the water diffusion problem. The first equation of the PDEs system (Eq. 1) is derived from Fick's law and it is supplemented by a term of the Soret effect. The second PDE (2) is derived from Fourier's law for transient thermal conduction. For the purposes of this study, the heat propagation is propelled only by the temperature gradient, the Duffour effect is neglected for its non-significant influence,

$$\frac{\partial M}{\partial t} - \nabla \cdot (\mathbf{D}\nabla M + s\mathbf{D}\nabla T) = 0 \quad (1)$$

$$\rho C \frac{\partial T}{\partial t} - \nabla \cdot \boldsymbol{\lambda}\nabla T = 0 \quad (2)$$

where M is the actual moisture content (%), t is the time (s), D is the diffusion coefficients in the matrix (m^2/s), s is the Soret effect coefficient (1/K), T is the actual temperature (K), ρ is the density (g/cm^3), C is the specific heat (J/kg·K), and $\boldsymbol{\lambda}$ is the thermal conductivity coefficients matrix (W/m·K).

Applied boundary conditions, for moisture field (Eq. 3) and for thermal field (Eq. 4), are obtained from the heat and moisture transfer between the timber surfaces and the drying ambient (air). The boundary conditions are affected by the air velocity, which is considered in coefficients of heat and moisture transfer. These coefficients are invariable, induced in accordance with Siau (1995) and Horáček (2004) (pertaining to air velocity v_{air} = 1.5 m/s),

$$-\mathbf{n} \cdot (\mathbf{D}\nabla M + s\mathbf{D}\nabla T) = \alpha_M (M_{\partial\Omega} - EMC) \quad (3)$$

$$-\mathbf{n} \cdot \boldsymbol{\lambda} \nabla T = \alpha_T (M_{\partial\Omega} - T_{air}) \quad (4)$$

where n is the normal vector, α_M is the moisture transfer coefficient (m^2/s), $M_{\partial\Omega}$ is the boundary moisture content, *EMC* is the equilibrium moisture content, α_T is the heat transfer coefficient (W/mK), $T_{\partial\Omega}$ is the boundary temperature (K), and T_{air} is the air temperature (K).

Material Coefficients Definition

Material coefficients were defined as functions of moisture content and temperature. All of them were computed for every combination of moisture content values belonging to the interval $M \in \langle 0; 0.3 \rangle$ and temperature values from interval $T \in \langle 280; 380 \rangle$. An analytical determination of all the material coefficients used in the most nonlinear numerical model *B3* (Table 1) is presented below. The material coefficients and ambient parameters used in all four models are listed in Table 2.

Table 2. Ambient Parameters and Material Coefficients Used in Solved Numerical Models

	A	***B*$_1$**	***B*$_2$**	***B*$_3$**	**Units**
Ambient Parameters					
φ	φ *(t)*				(-)
T_{air}	353				(K)
EMC	*EMC (t)*				(-)
Material Coefficients					
M_0	0.25				(-)
T_0	293				(K)
ρ_0	420				(g/cm^3)
ρ_M	420	ρ_M *(M)*	ρ_M *(M)*	ρ_M *(M)*	(g/cm^3)
C	1535	*C (M, T)*	*C (M, T)*	*C (M, T)*	(J/kgK)
D_T	$4.87 \cdot 10^{-8}$	D_T *(M, T)*	D_T *(M, T)*	D_T *(M, T)*	(m^2/s)
D_L	$1.12 \cdot 10^{-9}$	D_L *(M, T)*	D_L *(M, T)*	D_L *(M, T)*	(m^2/s)
D_R	$1.68 \cdot 10^{-9}$	D_R *(M, T)*	D_R *(M, T)*	D_R *(M, T)*	(m^2/s)
λ_T	0.52	λ_T *(M, T)*	λ_W *(M, T)*	λ_T *(M, T)*	(W/mK)
λ_L	0.20	λ_L *(M, T)*	λ_L *(M, T)*	λ_L *(M, T)*	(W/mK)
λ_R	0.31	λ_R *(M, T)*	λ_R *(M, T)*	λ_R *(M, T)*	(W/mK)
s	-	-	0.222	*s (M, T)*	(1/K)
α_M	$5 \cdot 10^{-7}$				(m/s)
α_T	20				(W/m^{2}K)

Water diffusion coefficients

The water diffusion coefficients were computed separately for tangential (Eq. 5), longitudinal (Eq. 6), and radial (Eq. 7) directions. The computation of diffusion coefficients was based on formulas given by Siau (1995). Radial diffusion coefficient is 1.5× higher than the tangential diffusion coefficient (Trcala 2012),

$$D_T = \left(\frac{1}{1-P_M}\right) \cdot \left(\frac{D_{BT} \cdot D_V}{D_{BT} + D_V \cdot \left(1-\sqrt{P_M}\right)}\right) \quad (5)$$

$$D_L = \left(\frac{P_M}{1-P_M}\right) \cdot \left(\frac{D_V \cdot D_{BL}}{D_{BL} + 0.01 \cdot \left(1-\sqrt{P_M}\right) \cdot D_V}\right) \quad (6)$$

$$D_R = 1.5 \cdot D_T \quad (7)$$

where D_T, D_L, and D_R are the diffusion coefficients for tangential, longitudinal, and radial direction (m^2/s), respectively, P_M is the wood porosity (-), D_{BT} and D_{BL} are the cell wall longitudinal and tangential diffusion coefficients (m^2/s), respectively, and D_V is the diffusion coefficient of water vapor in the cell lumen (m^2/s).

Computations are based on Siau's analytical model of water diffusion coefficients (Siau 1984), which was experimentally verified by Čermák and Trcala (2012). The formulas for diffusion coefficients computation are respecting two kinds of microstructural water motion– the diffusion in cell wall (Eqs. 8 and 9) and the diffusion in the cell lumen (Eq. 10). These formulas describe the longitudinal and transversal water diffusion in the cell wall. The value of longitudinal diffusion coefficient is higher than the value of the transversal one. This is caused by the divergent fibrillar structure of the cell wall in longitudinal and transversal directions (micro- and sub-microcapillaries oriented lengthwise with the cell wall axis) (Horáček 2004). Microstructural diffusion coefficients D_{BT}, D_{BL}, and D_V are nonlinear, affected by actual moisture content and temperature,

$$D_{BT} = 7 \cdot 10^{-6} \cdot e^{\frac{-E_a}{RT}} \quad (8)$$

$$D_{BL} = 2.5 \cdot D_{BT} \quad (9)$$

$$D_V = D_a \cdot \frac{0.018 \cdot p_0}{\rho_{BS} \cdot RT} \cdot \frac{\partial \varphi}{\partial M} \quad (10)$$

where e is the Euler's number (e = 2.71828), E_a is the activation energy of bound water (J/mol), R is the gas constant (R = 8.3144 J/Kmol), D_a is the air water vapor diffusion coefficient (m^2/s), p_0 is the saturated water vapor pressure (Pa), ρ_{BS} is the wood substance reduced density (g/cm^3), and φ is the relative air humidity (-).

The activation energy of bound water in wood (Eq. 11) represents the influence of the actual moisture content on the cell wall diffusion coefficient (Skaar 1988).

$$E_a = 38500 - 29000M \quad (11)$$

The diffusion coefficient in cell lumen is based on the Dushman's equation for water vapor diffusion in air (Eq. 12) (Dushman and Lafferty 1962). The dependence of cell lumen diffusion coefficient on temperature and moisture content is considered in formulas for saturated water vapor pressure (from Kirchhoff's equation) (Siau 1995) (Eq. 13), reduced density of wood substance (Eq. 14), and RH (derived from DeBoer-Zwicker's isotherm equation) (Eq. 15) (Siau 1995; Horáček 2004). The DeBoer-Zwicker's coefficients for *Picea sitchensis* A (Eq. 16) and B (Eq. 17) were used to apply the temperature effect on RH computation (Horáček 2004). The used coefficient offers a sufficient approximation for wood of *Picea abies* (Babiak 1990),

$$D_a = \frac{2.2}{p_{atm}} \left(\frac{T}{273.15}\right)^{1.75} \quad D_a = \frac{2{,}2}{p_{atm}} \cdot \left(\frac{T}{273{,}15}\right)^{1{,}75} \quad (12)$$

$$p_0 = e^{53.421 - \frac{6516.3}{T} - 4.125 \cdot lnT} \quad (13)$$

$$\rho_{BS} = \frac{\rho_S}{1 + \rho_S M} \quad (14)$$

$$\varphi = e^{-Ae^{-BM}} \quad (15)$$

$$A = 7.7317006 - 0.014348T \quad (16)$$

$$B = 0.008746 + 0.000567T \quad (17)$$

where p_{atm} is the standard atmospheric pressure (p_{atm} = 101330 Pa), ρ_s is the wood substance density (ρ_s = 1500 g/cm^3), and A and B are the DeBoer-Zwicker's coefficients (-).

After the value of microstructural water diffusion coefficients, the next property that affects the diffusion coefficients is the wood porosity (Eq. 18). Wood porosity is dependent on the convective wood density (Eq. 19), which is the converted value of the dry wood density,

$$P_M = 1 - \rho_k \cdot \left(\frac{1}{\rho_s} + M\right) P_M = 1 - \rho_k \cdot \left(\frac{1}{\rho_s} + M\right) \quad (18)$$

$$\rho_k = \frac{\rho_0}{1+0.28\rho_0} \quad (19)$$

where ρ_k is the conventional density (g/cm^3) and ρ_0 is the dry wood density (g/cm^3).

The described theorems were applied for diffusion coefficients computation. The dependence of computed diffusion coefficients on temperature and moisture content is displayed in Fig. 3.

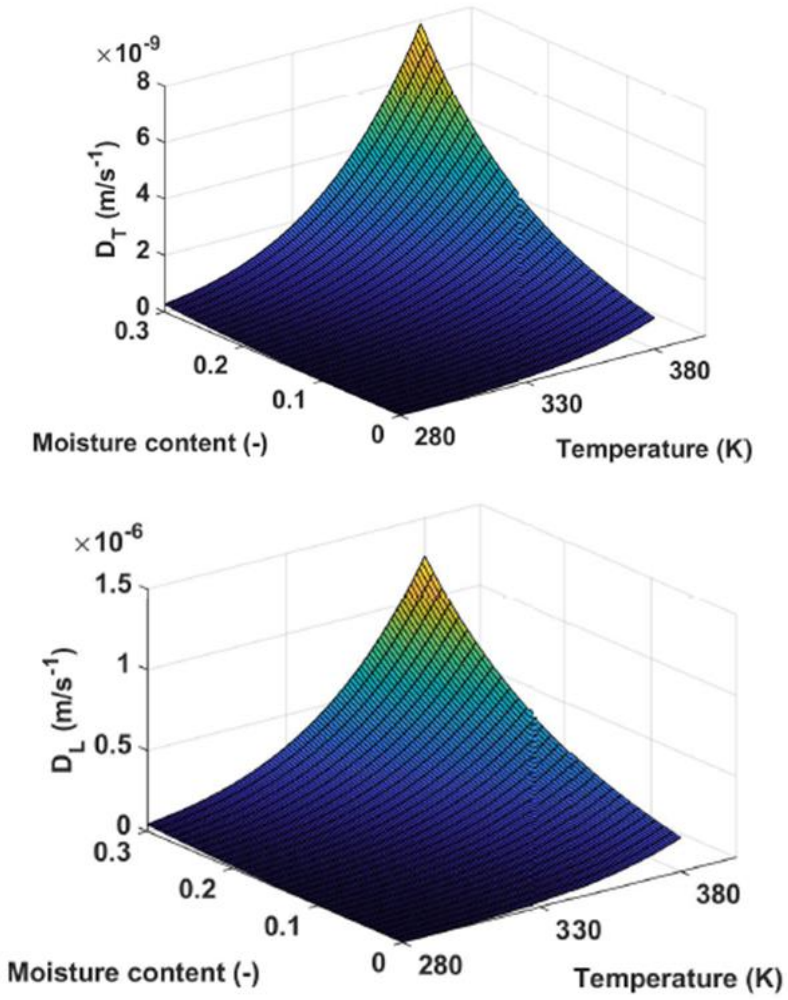

Fig. 3. Tangential and longitudinal water-diffusion coefficients' dependence on temperature and moisture content

Thermal conductivity coefficients

The thermal conductivity of wood is affected by its density, wood porosity, temperature, and moisture content. MacLean (1941) specified the equation (Eq. 20) for thermal conductivity of wood in the tangential direction. The thermal conductivity coefficients for radial (Eq. 21) and longitudinal (Eq. 22) directions gain 1.5× (R) and 2.5× (L) higher values than the tangential coefficient. In MacLean's equation, there is a coefficient *a*, which is specified as $a = 0.004$ for $M < 40\%$. The dependence of the thermal conductivity on the temperature was described as a linear function by Siau (1995) (Eq. 23).

Figure 4 presents the dependence of thermal conductivity in the tangential direction on temperature and moisture content,

$$\lambda_T = \rho_k \cdot (0.217 + a \cdot M) + 0.024 \cdot P_M \quad (20)$$

$$\lambda_R = 1.5 \cdot \lambda_T \quad (21)$$

$$\lambda_L = 2.5 \cdot \lambda_T \quad (22)$$

$$\lambda = \lambda_i\big(1 + 0.004 \cdot (T - 303)\big) \quad (23)$$

where λ_T, λ_R, and λ_T are the thermal conductivity coefficients (W/mK), and a is the coefficient for thermal conductivity determination (for $M < 0.4$, $a = 0.004$).

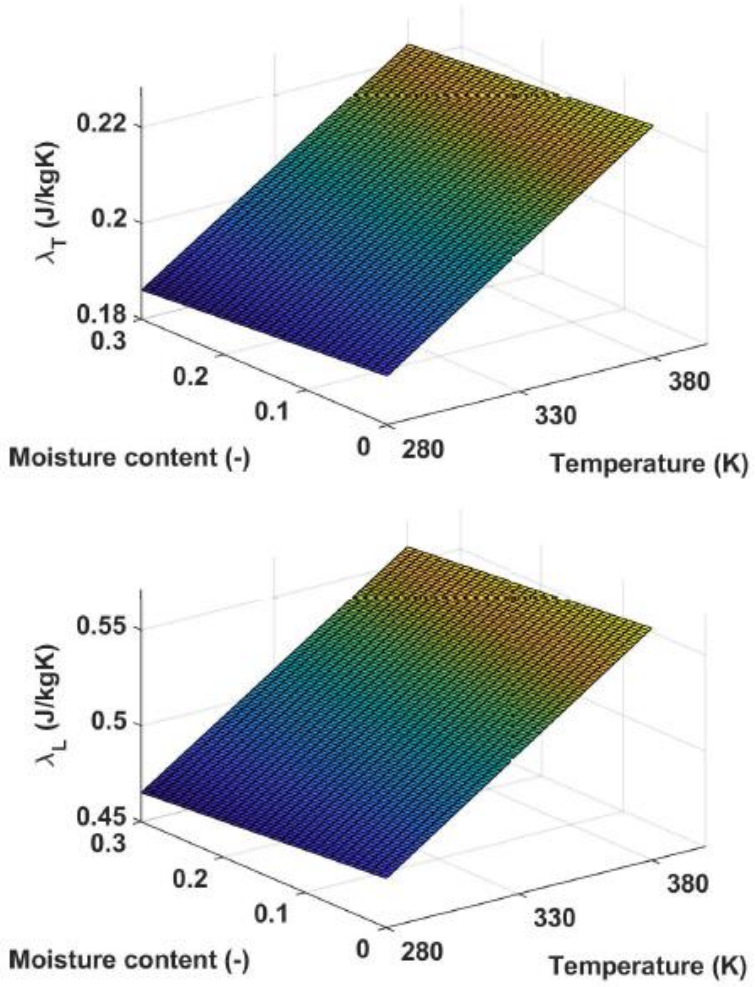

Fig. 4. Tangential and longitudinal thermal conductivity coefficient's dependence on temperature and moisture content

Specific heat

In the same way as previous material coefficients, the specific heat coefficient is a variable dependent on temperature and moisture content (Fig. 5). The formulas (Eqs. 24 and 25) defined by Skaar (1988) were used for specific heat calculations. Skaar's definition of specific heat is valid for temperatures lower than 100 °C and for a moisture content lower than the fiber saturation point (ca 30%),

$$C_0 = 1117 + 4.87 \cdot (T - 273.15) \quad (24)$$

$$C_M = \frac{C_0 + MC_W}{1+M} \quad (25)$$

where C_0 is the specific heat of dry wood (J/kgK), C_M is the specific heat of wood with actual moisture M (J/kgK), and C_W is the specific heat of water (J/kgK).

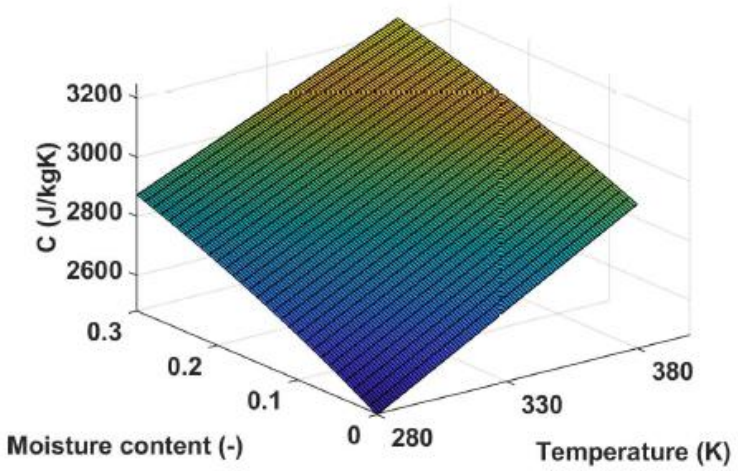

Fig. 5. The dependence of specific heat coefficient on temperature and moisture content

Density

All of the simulations described in this paper were realized for wood of *Picea abies*. In the task of coupled moisture and heat transfer computations, the differences of the wood species is mainly expressed by its density. In this case, the density value of dried wood was ρ_0 = 420 g/cm^3. For numerical simulations, the density (Eq. 26) was defined as a function of moisture content. The following Kollmann's equation (Kollmann 1951) is valid for moisture content lower than fiber saturation point and can be used with the assumption of the linear dependence of shrinkage on moisture content,

$$\rho_M = \rho_0 \cdot \frac{1+M}{1+0.993 \cdot \rho_0 \cdot M} \quad (26)$$

where ρ_k is the density of wood with actual moisture M (g/cm^3).

Soret effect coefficient

The Soret effect coefficient (Eq. 27) reflects moisture flux incurred by the thermal gradient (Siau 1984; Avramidis *et al.* 1992b). It is based on the slope of the sorption isotherms and the activation energy for water-diffusion E_a (Eq. 11). The *EMC* is a function of relative humidity and the temperature (Eq. 28). The Soret effect decreases with the increase of moisture and with the increase of temperature (Fig. 6):

$$s = \frac{\varphi}{RT} \cdot \frac{\partial EMC}{\partial \varphi} \cdot \frac{E_a}{T} \quad (27)$$

$$EMC(\varphi, T) = \frac{1}{B} \cdot ln \frac{A}{ln\frac{1}{\varphi}} \quad (28)$$

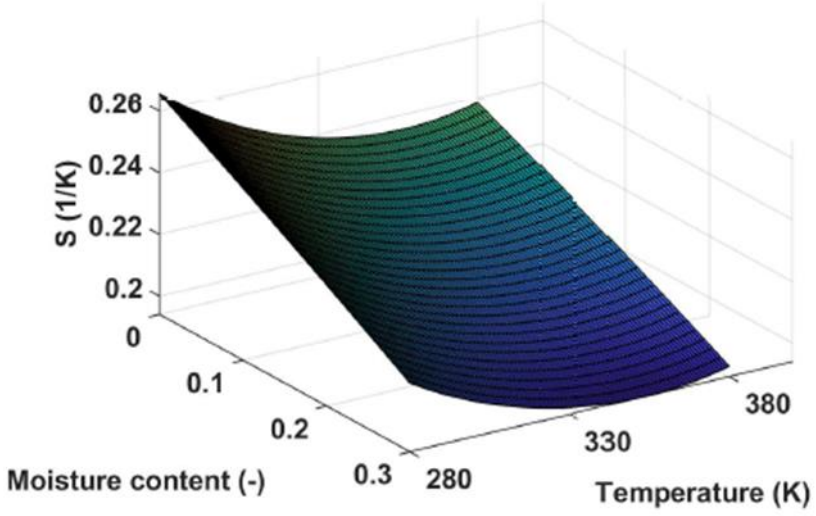

Fig. 6. The dependence of Soret effect coefficient on temperature and moisture content

Implementation to the FEM Solver

Numerical simulations are performed by FEM solver *COMSOL Multiphysics*, which allows conventional physics-based user interfaces and coupled systems of PDEs. This software offers a wide range of interfaces for solving varied physical tasks. In this case, the PDEs system was inputted to the 'Coefficient form PDE interface' with two variables – *M* and *T*. The predefined equation (Eq. 29) is below,

$$e_a \frac{\partial^2 u}{\partial t^2} + d_a \frac{\partial u}{\partial t} + (-c\nabla u - \alpha u + \gamma) + \beta \nabla u + au = f \quad (29)$$

$$\mathbf{u} = [\mathrm{M}, \mathrm{T}]^T \qquad \nabla = \left[\frac{\partial}{\partial x}, \frac{\partial}{\partial y}, \frac{\partial}{\partial z}\right]$$

where e_a, d_a, c, α, γ, β, a, and f are the matrices of coefficients dependent on time, direction (x, y, z), or u.

The vector function u has two components, *M* and *T*. Coefficients c and d_a were defined as matrices (Eq. 30) consisting from submatrices (Eq. 31) belonging to defined system of PDEs (Eq. 32) and (Eq. 33):

$$\mathbf{u} = \begin{pmatrix} M \\ T \end{pmatrix}, \quad \mathbf{c} = \begin{pmatrix} \mathbf{D} & s\mathbf{D} \\ 0 & \boldsymbol{\lambda} \end{pmatrix}, \quad \mathbf{d}_a = \begin{pmatrix} 1 & 0 \\ 0 & c\rho_M \end{pmatrix}$$

$$\mathbf{u} = \begin{pmatrix} M \\ T \end{pmatrix}, \quad \mathbf{c} = \begin{pmatrix} \mathbf{D} & s\mathbf{D} \\ 0 & \boldsymbol{\lambda} \end{pmatrix}, \quad \mathbf{d}_a = \begin{pmatrix} 1 & 0 \\ 0 & c\rho_M \end{pmatrix}$$

(30)

$$\mathbf{D} = \begin{pmatrix} D_T & 0 & 0 \\ 0 & D_L & 0 \\ 0 & 0 & D_R \end{pmatrix}, s\mathbf{D} = \begin{pmatrix} sD_T & 0 & 0 \\ 0 & sD_L & 0 \\ 0 & 0 & sD_R \end{pmatrix}, \boldsymbol{\lambda} = \begin{pmatrix} \lambda_T & 0 & 0 \\ 0 & \lambda_L & 0 \\ 0 & 0 & \lambda_R \end{pmatrix} \quad (31)$$

The boundary conditions were specified into a predefined equation (Eq. 32) ('Flux/Source' in 'COMSOL'), which belongs to the general PDE above (Eq. 29). The right side of the equation describes a boundary condition of the third type, where g and q are matrices (Eq. 33) and (Eq. 34) based on boundary condition equations:

$$-\mathbf{n}\cdot(-c\nabla\mathbf{u}-\alpha\mathbf{u}+\gamma)=g-q\mathbf{u} \qquad (32)$$

$$\mathbf{u}=[M,T]^T \quad \nabla=\left[\frac{\partial}{\partial x},\frac{\partial}{\partial y},\frac{\partial}{\partial z}\right]$$

$$g=\begin{pmatrix}\alpha_M EMC\\ \alpha_T T_{air}\end{pmatrix} \qquad (33)$$

$$q=\begin{pmatrix}\alpha_M & 0\\ 0 & \alpha_T\end{pmatrix} \qquad (34)$$

The geometry of the solid block was meshed using structural mesh of pentahedrons with a minimal size of 0.015 m and maximal size of 0.02 m (Fig. 7). The number of elements was 3817 and their average quality was 91 %. The solution was realized as a time-dependent nonlinear task with a time step of 300 s (636 steps). Integrated 'COMSOL's' solver 'MUMPS' was used.

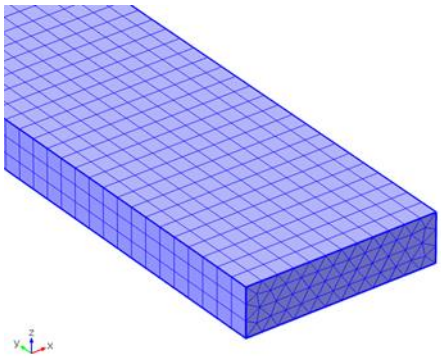

Fig. 7. Mesh application on geometrical body

RESULTS AND DISCUSSION

Thermal Field

The temperature in the timber is non-uniform only in the first phase of drying when the timber is heated up. In the next phases the thermal field is constant because of zero temperature gradient. Figure 8 represents results from four numerical simulations and the prediction given by the common standard. The question was – when is the uniform temperature gained? Results from models *A* and *B3* predict the uniform temperature after 3 h, and B_1 and B_2 after 4 h. The standard ON 49 0651 (1989) predicts that not frozen timber reaches the uniform drying temperature at a rate of 1 h per 1 cm of thickness (in this task 5 cm = 5 h).

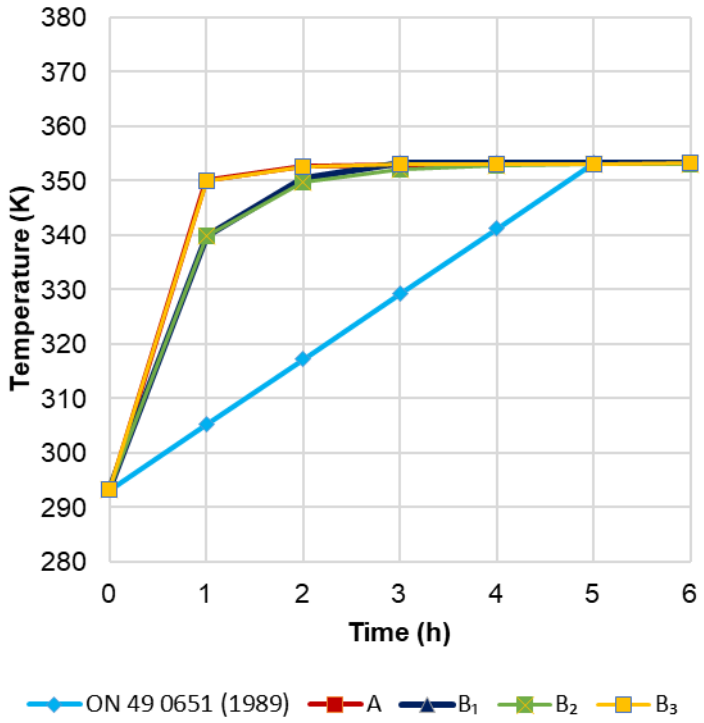

Fig. 8. Timber heating phase of drying process – four numerical solutions and prediction from common standard

Generally, the authors can say that nonlinearities have an insignificant influence on heating phase duration, because the linear model *A* and the most nonlinear model B_3 gained uniform temperature in the same time, while the other two models B_1 (nonlinear without Soret effect) and B_2 (nonlinear with constant Soret effect) assumed slower warming of timber.

The other question was the eventual influence of the nonlinear heat transfer coefficient, which was constant in the authors' simulations. This is the task for sensitivity analysis or the next set of computations with the nonlinear heat transfer coefficient.

Moisture Field

The results of moisture content change during kiln-drying were observed in four points and on the middle plane, as specified in Fig. 1. The average moisture content in a solid body was observed and compared with presumptions given by the commonly used standard.

Table 3. Simulations Results After 3 h of Drying (End of Heating Phase)

	A	***B*$_1$**	***B*$_2$**	***B*$_3$**
Middle (1)	25.0%	24.9%	27.8%	27.4%
Lengthwise Edge Middle Point (2)	10.1%	10.1%	9.0%	9.1%
XY-surface Middle (3)	14.5%	15.6%	12.9%	13.3%
Corner Point (4)	9.7%	9.5%	8.3%	8.4%

The four points solutions are displayed in Fig. 9 The biggest differences between all these points were found in the heating phase (0 to 3 h). Differences during the drying phase (3 to 53 h) were minor. The water transfer from boundary layers into the middle parts during the heating phase was found. This was caused by a higher influence of temperature gradient than moisture content gradient on moisture field during this phase. The most nonlinear simulation B_3 shows minor influence of the Soret effect compared to the simulation with constant value of the Soret effect coefficient (B_2), which is probably caused by the significant evolution of thermal gradient during heating phase. The thermodiffusion coefficient *s* is highly dependent on the thermal gradient and it is not clear to use this coefficient as a constant value. It is obvious that in case of models B_2 and B_3 in all observed points the moisture content reaches the turning point during the heating phase. The turning point is gained instantly with reaching the thermal equilibrium (zero thermal gradient) in the observed point. From that moment the moisture field is influenced by moisture content gradient only.

The moisture contents at the end of the heating phase are stated in Table 3. The highest differences in this time were in the middle point. The difference between B_1 and B_3 reached 2.85%. The results of models B_2 and B_3 were compared to modelling and experimental results of Avramidis *et al.* (1992a), and it can be stated that the shapes of moisture-loss curves correspond to their results.

Moisture decrease differences were also evident during the drying phase. These differences were obvious especially in the middle point, where simulation *A* predicted slower moisture decrease compared to the results from nonlinear models. Insignificant differences were found in moisture content change during the drying phase in the middle of the boundary surface. Table 4 presents the moisture contents at 53 h (final time). The differences at the final time were minor compared to the differences at the end of the heating phase. The biggest difference in the final time was found in the middle point, between the results from *A* and B_1 simulations (0.49%).

Table 4. Moisture Content in Observed Points at the End of Drying (53 h)

	A	***B*$_1$**	***B*$_2$**	***B*$_3$**
Middle (1)	14.5%	14.0%	14.4%	14.3%
Lengthwise Edge Middle Point (2)	4.0%	4.0%	3.9%	3.9%
XY-surface Middle (3)	5.8%	5.6%	5.7%	5.6%
Corner Point (4)	4.0%	3.9%	3.9%	3.9%

Moisture distributions at the *xz*-middle plane from the simulations are depicted in Fig. 10. These distributions differed primarily during the heating phase. Simulations *A* and B_1 predicted slower moisture content decrease in boundary layers than the simulations B_2 and B_3, which is caused by missing Soret effect in first two models. It is possible to observe differences in the middle parts drying throughout the process. This raise from the different moisture transport during the heating phase. Slower drying predicted by model *A* is caused by the constant values of material parameters, which are not changing with decreasing moisture content.

The values of average moisture content predicted by the assembled theoretical models are compared with the data given by the drying schedule from the commonly used standard ON 49 0651 (1989) (Fig. 11, Table 5). The maximal difference between simulations and the standard was 5.68% (at 10 h). The total differences between

simulations did not exceed 1.38%. From 0 h to 34 h, the simulations predicted faster drying than the standard features. The trend reverted in the last third of scheduled time and the simulations predicted slower moisture decrease. At the end of the drying process, the models predicted an average moisture content from 10.07% to 10.48% and the standard features desired 8%.

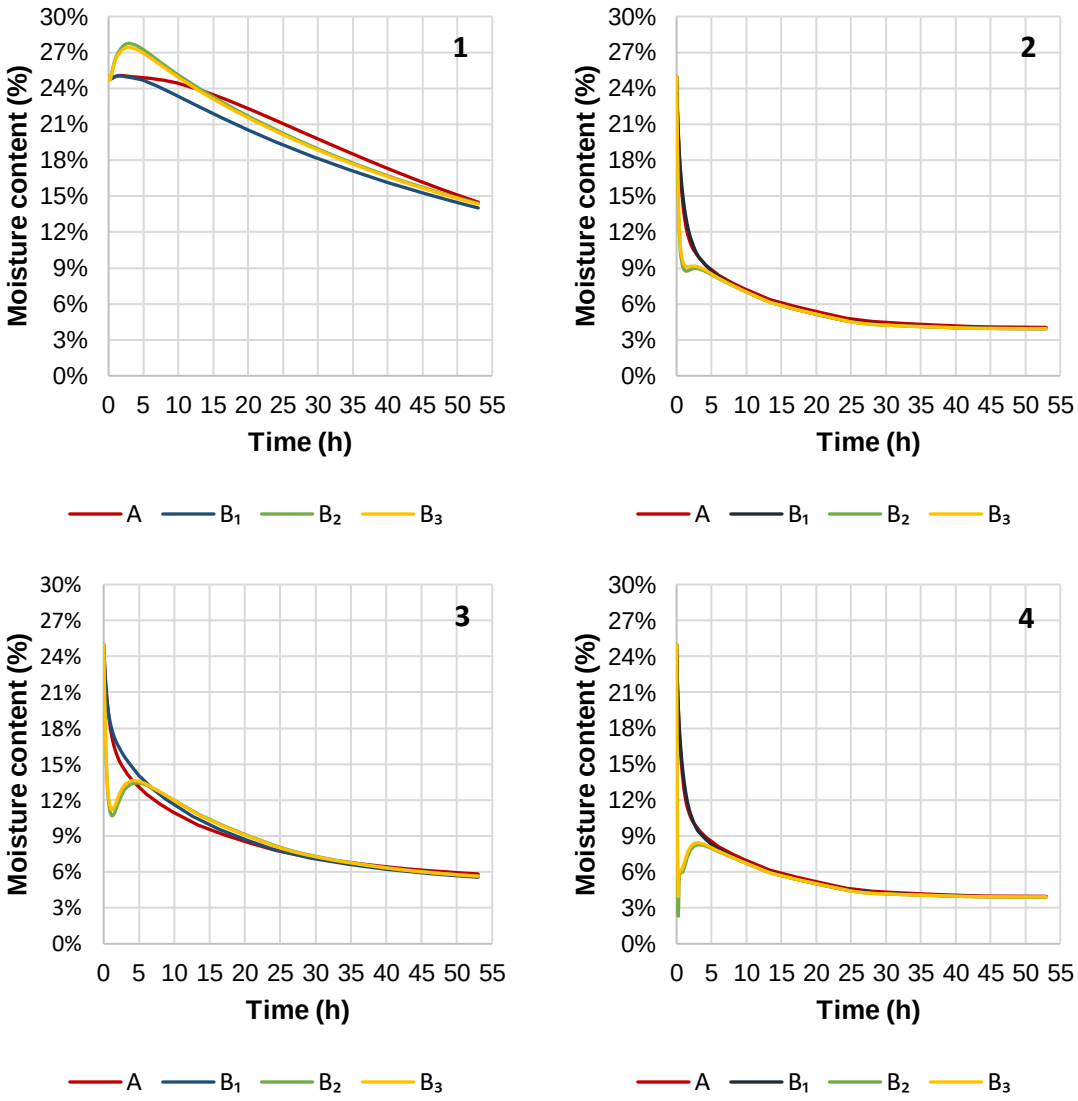

Fig. 9. Computed moisture content change during drying process in points 1, 2, 3, and 4

From the above discussed results stems that the choice of the nonlinearity level of input parameters, and the choice of coupling method depend on the specific example which is to be solved. If the goal is to obtain only the final moisture content, then the linear model is enough, as stated also in work of Eriksson *et al*. (2006). In case of the computation of the moisture content distribution in various times, which can be used as an initial study for drying stresses and cracks development analysis, it will be required to apply wood parameters dependent on actual moisture content and temperature. The thermodiffusion effect should be considered in case of drying schedules with high temperature gradients,

for example when modelling high temperature drying (Čermák *et al.* 2014) or heat treatment processes of wood.

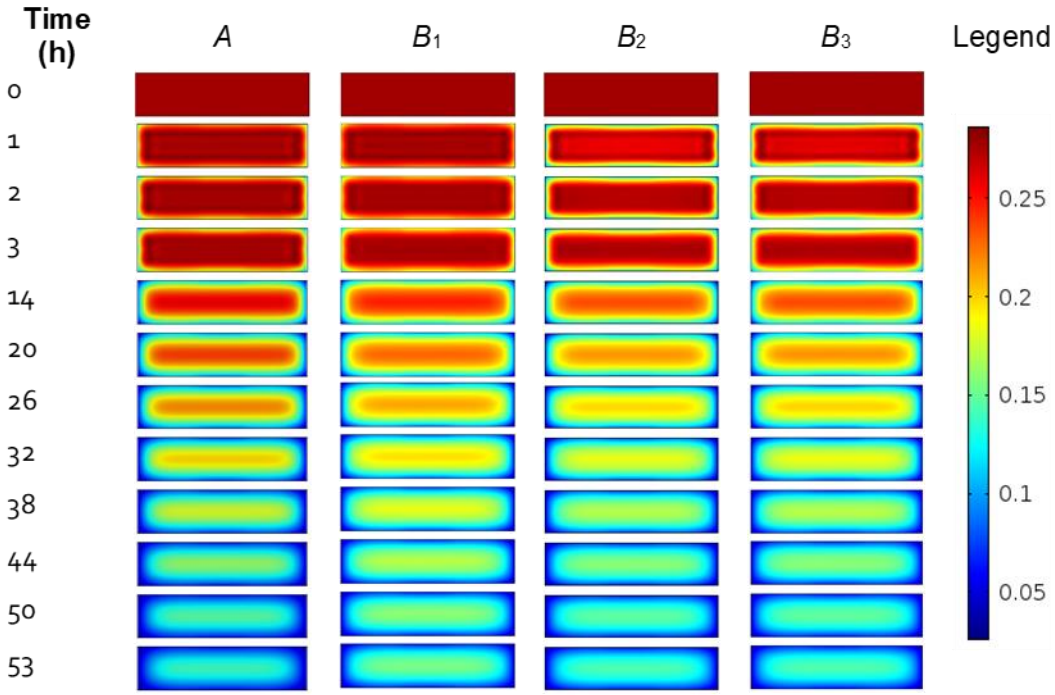

Fig. 10. Moisture distribution progress during kiln-drying of timber (computed by models *A*, B_1, B_2, and B_3)

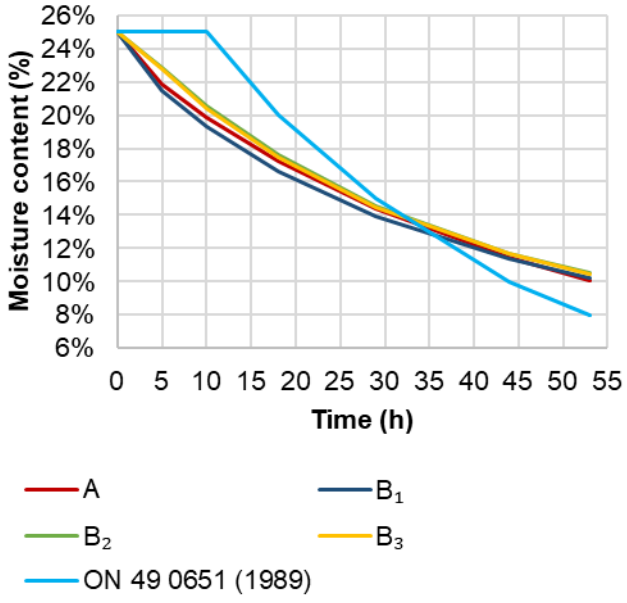

Fig. 11. Average moisture content during drying predicted by simulations and standard

Table 5. Average Moisture during Drying Process Predicted by Simulations and Standard for Kiln-drying

Time (h)	*A*	B_1	B_2	B_3	Standard ON 49 0651 (1989)
0	25.0%	25.0%	25.0%	25.0%	25.0%
5	21.9%	21.5%	22.9%	22.8%	25.0%
10	19.8%	19.3%	20.5%	20.4%	25.0%
18	17.2%	16.7%	17.6%	17.5%	20.0%
29	14.3%	13.9%	14.6%	14.5%	15.0%
44	11.4%	11.4%	11.7%	11.6%	10.0%
53	10.1%	10.2%	10.5%	10.4%	8.0%

CONCLUSIONS

1. The influence of nonlinearities on the results of wood kiln-drying numerical simulations was observed. Four different unsteady-state numerical models were developed and compared with each other and to the commonly used standard for kiln-drying of wood.
2. The linear model was sufficiently precise only for describing the average moisture content in the timber. To find out the moisture in various points in timber, it was better to use more nonlinear models with material parameters dependent on time-dependent moisture content and temperature and coupled by Soret effect.
3. It was discovered that the Soret effect had no impact on the total drying time, but it non-negligibly affected the moisture layout in the time of warming the timber. The constant Soret effect coefficient had a more significant effect than the Soret effect coefficient, as the variable was dependent on moisture and temperature. There was a higher increase of moisture in the middle point of the timber and higher decrease of moisture in the surface layers, in comparison to the model with variable Soret effect coefficients during warming of the timber, in the model with the constant Soret effect.
4. Higher differences were found between the flow of moisture during the drying process pretended by models and the standard. The model's average moisture in the timber differed from the average moisture defined by the standard during the entire time of the drying process. The standard defined final moisture at the end of the process was 2.31% less than the final moisture computed by the numerical models.

ACKNOWLEDGMENTS

The manuscript was supported by the Specific University Research Fund of the FFWT Mendel University in Brno, Czech Republic, Project LDF_VP_2018004.

REFERENCES CITED

Avramidis, S., Englezos, P., and Papathanasiou, T. (1992a). "Dynamic nonisothermal transport in hygroscopic porous media: Moisture diffusion in wood," *AIChE Journal* 38(8), 1279–1287. DOI: 10.1002/aic.690380813

Avramidis, S., Siau, J. F., and Hatzikiriakos, S. G. (1992b). "An irreversible thermodynamics model for unsteady-state nonisothermal moisture diffusion in wood," *Wood Science and Technology* 28(5), 349-358. DOI: 10.1007/BF00195282

Babiak, M. (1990). *Wood Water System*, VŠLD, Zvolen, Slovakia.

Babiak, M. (1995). "Is Fick's law valid for the adsorption of water by wood?," *Wood Science and Technology* 29(3), 227-229. DOI: 10.1007/BF00204590

Čermák, P., and Trcala, M. (2012). "Influence of uncertainty in diffusion coefficients on moisture field during wood drying," *International Journal of Heat and Mass Transfer* 55(25–26), 7709-7717. DOI: 10.1016/j.ijheatmasstransfer.2012.07.070

Čermák, P., Horáček, P. and Rademacher, P. (2013). "Measured temperature and moisture profiles during thermal modification of beech (*Fagus sylvatica L.)* and spruce (*Picea abies L.* Karst) wood. *Holzforschung* 68(2), 175-183. DOI: 10.1515/hf-2013-0047

Dushman, S., and Lafferty, J. M. (1962). *Scientific Foundations of Vacuum Technique*, Wiley, New York, NY, USA.

Eitelberger, J., and Hofstetter, K. (2011). "A comprehensive model for transient moisture transport in wood below the fiber saturation point: Physical background, implementation and experimental validation," *International Journal of Thermal Sciences* 50(10), 1861-1866. DOI: 10.1016/j.ijthermalsci.2011.02.024

Elustondo, D., and Oliveira, L. (2006). "Opportunities to reduce energy consumption in softwood lumber drying," *Drying Technology* 24(5), 653-662. DOI: 10.1080/07373930600626644

Eriksson, J., Ormarsson, S., and Petersson, H. (2006). "Finite-element analysis of coupled nonlinear heat and moisture transfer in wood," *Numerical Heat Transfer, Part A: Applications* 50(9), 851-864. DOI: 10.1080/10407780600669282

Gebhart, B. (1993). *Heat Conduction and Mass Diffusion*, McGraw-Hill, New York, NY, USA.

He, Z.-b., Wang, Z.-y., Qian, J., and Yi, S.-l. (2019). "Modeling and simulation of heat-mass transfer and its application in wood thermal modification," *Results in Physics* 13, 102213, DOI: 10.1016/j.rinp.2019.102213

Horáček, P. (2004). *Model of Coupled Moisture and Thermal Fields during Wood Drying*, Habilitation Thesis, Mendel University in Brno, Brno, Czech Republic.

Jankowsky, I. P., and Gonçalves Luiz, M. (2006). "Review of wood drying research in Brazil: 1984-2004," *Drying Technology* 24(4), 447-455. DOI: 10.1080/07373930600611893

Kang, W., Chung, W. Y., Eom, C. D., and Yeo, H. (2008). "Some considerations in heterogeneous nonisothermal transport models for wood: A numerical study," *Journal of Wood Science* 54(4), 267-277. DOI: 10.1007/s10086-007-0938-0

Klement, I., and Detvaj, J. (2007). *Technológia Prvostupňového Spracovania Dreva [Technology of Primary Wood Processing]*, Technical University in Zvolen, Zvolen, Slovakia.

Kocaefe, D., Younsi, R., Poncsak, S., and Kocaefe, Y. (2007). "Comparison of different models for the high-temperature heat-treatment of wood," *International Journal of*

Thermal Sciences 46(7), 707-716. DOI: 10.1016/j.ijthermalsci.2006.09.001

Kollmann, F. (1951). *Technologie des Holzes und der Holzwerkstoffe*, Springer, Berlin, Germany.

Lewis, R. W., and Ferguson, W. J. (1993). "A partially nonlinear finite element analysis of heat and mass transfer in a capillary-porous body under the influence of a pressure gradient," *Applied Mathematical Modelling* 17(1), 15-24. DOI: 10.1016/0307-904X(93)90123-X

Luikov, A. V. (1966). *Heat and Mass Transfer in Capillary-porous Bodies*, Pergamon Press, New York, NY, USA.

Luikov, A. V. (1980). *Heat and Mass Transfer*, Mir Publishers, Moscow, Russia.

MacLean, J. D. (1941). "Thermal conductivity of wood," *Heating, Piping and Air Conditioning* 13(6), 380–391.

Mitchell, P. (2019). "Development of an air drying index for lumber," *BioResources* 14(3), 6657-6665. DOI: 10.15376/biores.14.3.6657-6665

Nascimento, T. M., Monteiro, T. C., Baraúna, E. E. P., Moulin, J. C., and Azevedo, A. M. (2019). "Drying influence on the development of cracks in *Eucalyptus* logs," *BioResources* 14(1), 220-233. DOI: 10.15376/biores.14.1.220-233

Pang, S. (2004). "Optimizing airflow reversals for kiln drying of softwood timber by applying mathematical models," *Maderas. Ciencia y Tecnología* 6(2), 95-108. DOI: 10.4067/S0718-221X2004000200001

Pang, S. (2007). "Mathematical modeling of kiln drying of softwood timber: Model development, validation, and practical application," *Drying Technology* 25(3), 421-431. DOI: 10.1080/07373930601183751

Pérez-Pena, N., Chávez, C., Salinas, C., and Ananías, R. (2018). "Simulation of drying stresses in *Eucalyptus nitens* wood," *BioResources* 13(1), 1413-1424. DOI: 10.15376/biores.13.1.1413-1424

Perré, P., and Keey, R. B. (2007). "Drying of wood: Principles and practices," in: *Handbook of Industrial Drying*, A. S. Mujumdar (ed.), CRC Press, Taylor & Francis Group, Boca Raton, FL, USA, pp. 821–877.

ON 49 0651 (1989). "Timber kiln-drying," Czech Office for Standards, Metrology and Testing, Prague, Czech Republic.

Sherwood, T. K. (1929). "The drying of solids- I," *Industrial and Engineering Chemistry* 21(1), 12-16. DOI: 10.1021/ie50229a004

Siau, J. F. (1984). *Transport Processes in Wood*, Springer-Verlag, Berlin, Heidelberg, Germany.

Siau, J. F. (1992). "Nonisothermal diffusion model based on irreversible thermodynamics," *Wood Science and Technology* 26(5), 325-328. DOI: 10.1007/BF00226073

Siau, J. F. (1995). *Wood - Influence of Moisture on Physical Properties*, Virginia Polytechnic Institute and State University, Blacksburg, VA, USA.

Skaar, C. (1988). *Wood-water Relations*, Springer-Verlag, Berlin, Heidelberg, Germany.

Trcala, M. (2012). *Model of Coupled Moisture and Heat Transfer in Wood*, Ph.D. Thesis, Mendel University in Brno, Brno, Czech Republic.

Trcala, M. (2015). "Spectral stochastic modeling of uncertainties in nonlinear diffusion problems of moisture transfer in wood," *Applied Mathematical Modelling* 39(5–6), 1740–1748. DOI: 10.1016/j.apm.2014.09.032

Vergnaud, J. M. (1991). *Liquid Transport Processes in Polymeric Materials: Modelling and Industrial Applications*, Prentice Hall International Ltd., London, UK.

Whitaker, S. (1977). "Simultaneous heat, mass, and momentum transfer in porous media: A theory of drying," *Advances in Heat Transfer* 13, 119-203. DOI: 10.1016/S0065-2717(08)70223-5

Article submitted: June 4, 2019; Peer review completed: September 18, 2019; Revised version received: October 21, 2019; Accepted: October 23, 2019; Published: October 25, 2019.
DOI: 10.15376/biores.14.4.9786-9805